

The Sun's distance from the Galactic Centre and mid-plane, and the Galactic old bulge's morphology: 715 VVV Type II Cepheids

Evgeny Griv,¹★ Michael Gedalin,¹ Paweł Pietrukowicz,² Daniel Majaess^{3,4} and Ing-Guey Jiang^{5,6}

¹Department of Physics, Ben-Gurion University of the Negev, Beer-Sheva 8410501, Israel

²Astronomical Observatory, University of Warsaw, Al. Ujazdowskie 4, PL-00-478 Warszawa, Poland

³Department of Chemistry and Physics, Mount Saint Vincent University, Halifax, NS B3M 2J6, Canada

⁴Department of Astronomy and Physics, Saint Mary's University, Halifax, NS B3H 3C3, Canada

⁵Department of Physics and Institute of Astronomy, National Tsing-Hua University, Hsin-Chu 300, Taiwan

⁶Center for Informatics and Computation in Astronomy, National Tsing-Hua University, Hsin-Chu 300, Taiwan

Accepted 2021 February 2. Received 2021 February 1; in original form 2020 December 22

ABSTRACT

A statistical method is employed in tandem with new VISTA Variables in the Via Lactea (VVV) near-infrared observations to determine the Sun's distance from the Galactic Centre (r_0 , GC), the Sun's height from the local mid-plane (z_0), and to likewise infer the shape of the Galactic ~ 10 Gyr old bulge. Specifically, the conclusions stem from an investigation of 715 high-latitude ($|b| > 1^\circ$) and centrally symmetric concentrated Type II Cepheids (T2Cs) recently identified in the VVV survey by Braga et al. The analysis yields $r_0 = 8.35 \pm 0.10$ kpc and $z_0 = 10 \pm 2$ pc. The T2Cs distribution within the effective bulge radius $r_{\text{bulge}} = 2\text{--}3$ kpc is an ellipsoid exhibiting axial ratios of $\approx 1:0.7:0.6$, with the major axis inclined at an angle $\theta \approx -3^\circ$ to the Sun–GC sightline. T2Cs do not trace a prominent barred structure at distances > 1 kpc from the GC. A key conclusion is that analyses of independent optical and infrared Optical Gravitational Lensing Experiment (OGLE) and VVV observations yield consistent results (e.g. $r_0 > 8.0$ kpc and both observations display a comparable shape of an ellipsoid), thus providing a constrained and reduced systematic uncertainty.

Key words: Galaxy: bulge – Galaxy: fundamental parameters – Galaxy: kinematics and dynamics – Galaxy: structure.

1 INTRODUCTION

The density distribution of periodic variable RR Lyrae stars (RRLs) in the Galactic old bulge can be now mapped by long-term optical surveys like the Optical Gravitational Lensing Experiment (OGLE; Soszyński et al. 2014, 2019; Pietrukowicz 2020) and *Gaia* (Gaia Collaboration et al. 2018), and near-infrared surveys like the VISTA Variables in the Via Lactea (VVV) exploring the facilities of the 4.1-m Visible and Infrared Survey Telescope for Astronomy (VISTA; Minniti et al. 2010, 2017; Surrot et al. 2019). In the first part of the work (Griv et al. 2020), we have examined 16 221 high-latitude ($|b| \gtrsim 2^\circ$) RRLs identified in the OGLE-IV by Soszyński et al. (2014) and subsequently evaluated by Pietrukowicz et al. (2015). The bulge sample of stars with ages $\tau \gtrsim 10$ Gyr was analysed via a modified form of the statistical method advocated by Rastorguev et al. (1994), and the distance to the Galactic Centre (GC) r_0 , the power-law index α , and an ellipsoidal distribution were determined (major axis a , and two minor axes b and c). It was assumed that the distribution may not be spherically symmetric (i.e. $a \neq b \neq c$), and the major axis is not necessarily inclined at an angle $|\theta| \sim 0^\circ$ relative to the Sun–GC sightline.

In principle one can determine the distance from the Sun to the old bulge's structure using RRLs. However, Majaess (2010) emphasized that an accurate determination of r_0 is hindered by countless effects

that include an ambiguous extinction law, a bias for smaller values of r_0 because of a preferential sampling of variable stars toward the near side of the bulge owing to extinction, and an uncertainty in characterizing how a mean distance to the group of variable stars relates to r_0 . A partial solution to the problem is to examine whether consistency exists between independent data sets and variable stars, e.g. Type II Cepheids (T2Cs) and RRLs. For example, the infrared sample of ~ 4000 VISTA Variables in VVV RRLs identified by Majaess et al. (2018) may be utilized, which independently bolsters and complements the OGLE data. Furthermore, the VVV results of Braga et al. (2018, 2019, 2020) are pertinent, given they established an extensive catalogue of T2Cs. T2Cs are Population II stars traversing the instability strip with periods between 1 and 50 d. These old (> 10 Gyr), low-mass ($\sim 0.5 M_\odot$), typically metal-poor stars encompass the GC. T2Cs can be used as distance indicators because they adhere to a period–luminosity relation (e.g. Majaess, Turner & Lane 2009a). Moreover, the impact of metallicity on their near-infrared period–luminosity relations is comparably negligible. RRLs and T2Cs adhere to the same period–luminosity relations in the near-infrared bands (Braga et al. 2020). T2Cs are 1–5 mag brighter than RRLs, but not as numerous. Indeed, the bulge is estimated to contain at least ~ 1000 T2Cs and $\sim 70\,000$ RRLs (Soszyński et al. 2019). As a result the Braga et al. (2019) T2Cs sample may be more complete than certain RRLs catalogues, thereby allowing the innermost regions of the bulge to be investigated. Majaess, Turner & Lane (2009b) have attempted to derive r_0 using a much smaller sample of OGLE T2Cs in the bulge.

* E-mail: griv@bgu.ac.il

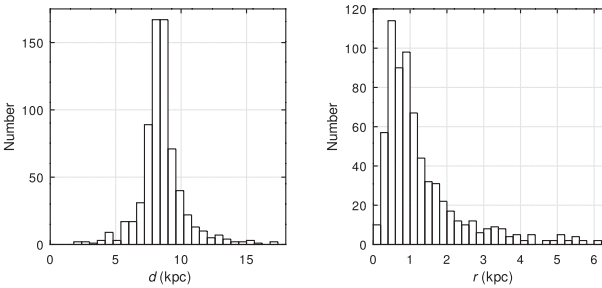


Figure 1. Distribution of all 715 T2Cs selected from the VVV survey of Braga et al. (2019) with respect to d and r (adopting $r_0 = 8.1$ kpc and $z_0 = 20$ pc).

A paradigm adopted to mitigate uncertainties is to analyse diverse samples of data tied to multiple passbands and standard candles. That approach is adopted in this study where new data from Braga et al. (2019) are employed to determine r_0 , and to characterize the bulge's morphology. A robust statistical method is applied to investigate the VVV data, and the results are compared to determinations inferred from OGLE. Consequently, various results can be compared and any consistency evaluated, namely by simultaneously leveraging the Pietrukowicz et al. (2015) OGLE V_{lc} RRLs data, the Majaess et al. (2018) VVV JHK_s RRLs data, and the Braga et al. (2020) VVV JHK_s T2Cs data. Moreover, an accurate determination of the Sun's height above the local Galactic mid-plane (z_0) can ensue.¹

In Section 2, selection of the data is described. Results of the model calculations are presented in Section 3. Section 4 contains the concluding remarks.

2 OBSERVATIONAL MATERIAL

Braga et al. (2019) published the most comprehensive up-to-date catalogue of T2Cs in the central regions of the Galaxy. The high-latitude ($|b| > 1^\circ$) VVV sample from Braga et al. (2019) features 715 objects with estimated distances from the Sun (d) and Galactic coordinates (ℓ, b ; not to be confused with the minor axis b of the observed ellipsoid of stars). The squared Galactocentric distance r of a star is given by

$$r^2 = (r_0 - d \cos b \cos \ell)^2 + d^2 \cos^2 b \sin^2 \ell + (d \sin b + z_0)^2.$$

Typical estimates for the quantities involved include $r_0 \approx 8.1$ kpc and $z_0 \approx 20$ pc (Bland-Hawthorn & Gerhard 2016; de Grijs & Bono 2016; Karim & Mamajek 2017; Yao, Manchester & Wang 2017; Camarillo et al. 2018; Reid et al. 2019). The distributions of stars relative to d and r are shown in Fig. 1. For regions of $r > 1$ kpc the stars exhibit a centrally concentrated distribution, and the spatial density of objects ρ can be described by a power law:

$$\rho \propto r^\alpha, \quad (1)$$

where the power-law index α is negative. The result relies on objects within $r = r_{\max}$ ranging from 2 to 4 kpc, and $r_0 = 8.1$ kpc and $z_0 = 20$ pc were assumed. Less than ≈ 10 per cent of all T2Cs lie beyond r_{\max} . The contribution of such distant objects to the likelihood function $L(r_0, \alpha, \theta, z_0, a, b, c)$ (equation 3 below) does not alter the conclusions.

Fig. 2 conveys the distribution of 715 T2Cs in a Cartesian XYZ

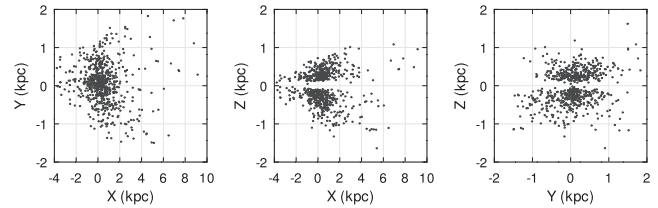


Figure 2. The distribution of 715 T2Cs in Cartesian XYZ coordinates and centred on the GC. The Sun at $(8.1, 0, 0.02)$, the X -axis points to the anticentre, the Y -axis points in the direction of Galactic rotation, and the Z -axis points upwards toward the North Galactic Pole. A spherical-like distribution and concentration around the GC are seen.

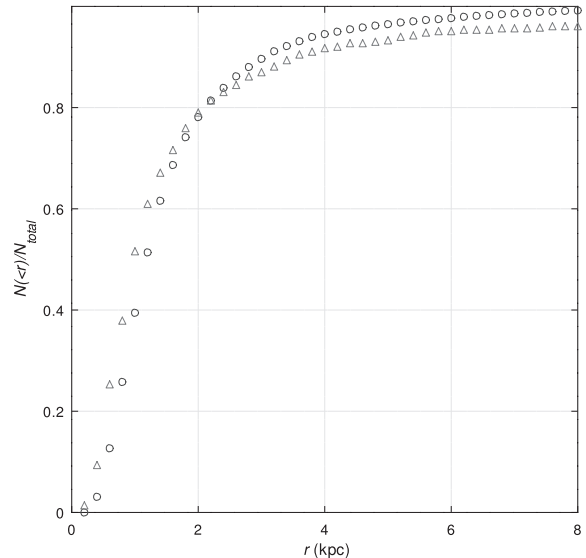


Figure 3. Normalized distribution for the VVV T2Cs (triangles) and OGLE RRLs (circles) populations. The half-population radius for both types of stars is $r_{hr} \approx 1.0$ kpc.

frame, where X increases towards the Galactic anticentre, Y increases along the direction of rotation of the Galaxy, and Z increases upwards out of the Galactic plane. A centrally symmetric, spherical-like spatial distribution and high concentration around the GC are readily discernible. The latter convincingly indicates that T2Cs do not belong to the disc population of the Galaxy (see also Dékány et al. 2013; Braga et al. 2018). Generally, the T2Cs of the bulge belong to the kinematically hot stellar population, with an ellipsoidal, centrally symmetric concentrated spatial distribution and with the velocity dispersions in the longitude and latitude directions of $\sigma v_\ell \approx \sigma v_b \approx 100 \text{ km s}^{-1}$; these stars have kinematics similar to RRLs (Braga et al. 2018). Fig. 2 also shows that the sample of objects populates almost all regions of the bulge well, thus presenting a complete picture of the distribution of stars in the old bulge. Regions close to the GC and the equatorial $Z = 0$ plane are not sampled. For $|Z| \lesssim 200$ pc dust extinction along the plane forces potential targets beyond the detection limit of the VVV and OGLE surveys. Dust extinction is proportional to $\cos \ell / \sin b$, and therefore the completeness of the sample drops (see also Rastorguev et al. 1994, for a discussion). That emphasizes why higher latitude VVV and OGLE objects were selected.

Following closely Navarro et al. (2021, fig. 6 therein), in Fig. 3 we display the normalized distribution of VVV T2Cs compared with that of the OGLE RRLs population. Both distributions show

¹The Milky Way hosts a stellar disc featuring an axial ratio of $\sim 1:10$, and the Solar system lies slightly above the plane toward the North Galactic Pole (e.g. Bland-Hawthorn & Gerhard 2016).

Table 1. The best model estimates inferred from the VVV T2Cs of Braga et al. (2019). Columns 1–9 highlight the following: the adopted bulge’s radius r_{bulge} , number of selected objects N inside r_{bulge} in the sample, solar distance r_0 , power-law index α , tilt angle θ , Sun’s distance from the mid-plane z_0 , normalized major axis of the symmetry of the ellipsoid a , minor axis b in the plane, and vertical axis c .

r_{bulge} (kpc)	N	r_0 (kpc)	α	θ ($^{\circ}$)	z_0 (pc)	a	b	c
2.0	565	8.35 ± 0.11	-2.5 ± 0.1	-3.5 ± 0.2	8 ± 2	1.0	0.7 ± 0.02	0.6 ± 0.03
2.5	596	8.35 ± 0.09	-2.7 ± 0.1	-2.5 ± 0.3	9 ± 2	1.0	0.7 ± 0.03	0.6 ± 0.02
3.0	622	8.35 ± 0.10	-2.7 ± 0.1	-1.7 ± 0.2	12 ± 3	1.0	0.6 ± 0.04	0.5 ± 0.03
3.5	642	8.35 ± 0.10	-2.8 ± 0.05	-3.3 ± 0.2	15 ± 3	1.0	0.5 ± 0.03	0.4 ± 0.04
4.0	656	8.35 ± 0.08	-3.0 ± 0.05	$+1.8 \pm 0.3$	16 ± 2	1.0	0.5 ± 0.03	0.4 ± 0.03

a convergence at $r = 3\text{--}4$ kpc. The half-population radius for both types of objects is almost the same, i.e. $r_{\text{hr}} \approx 1.0$ kpc. T2Cs and RRLs are almost equally concentrated. Interestingly, Navarro et al. (2021) found the radii containing half of the populations are $r_{\text{hr}} = 0.99, 0.61$, and 1.75 kpc for the compiled sample of $N = 64\,850$ RRLs from different surveys, red clump giants, and globular clusters, respectively. That is to say, relatively metal-rich red clump giants exhibit a more concentrated distribution.

The distribution of bulge VVV T2Cs and OGLE RRLs is similar, as inferred from Figs 1–3, and figs 1 and 2 from Griv et al. (2020). An average uncertainty of ± 5 per cent was adopted owing to the absence of individual distance uncertainties.

3 RESULTS OF CALCULATION

The methodology remains similar to that for our previous studies (Griv, Gedalin & Jiang 2019; Griv et al. 2020). The observed space distribution function of objects is

$$f(x, y, z) = A(r_0, \alpha, \theta, z_0, a, b, c)(r/\text{const})^\alpha, \quad (2)$$

where (x, y, z) are the Cartesian coordinates of objects, $z = 0$ for the Galactic mid-plane, the Sun is at $z > 0$, and the normalization factor A is to be found. Next, the likelihood function is in the following form:

$$L(r_0, \dots, c) = \prod_{i=1}^N f(r_i; r_0, \dots, c), \quad (3)$$

where N is the total number of objects. Finally, seven mutually independent parameters are constrained that maximize L , i.e. $r_0, \alpha, \theta, z_0, a, b$, and c .

The best model estimates are relayed in Table 1. Space distribution modelling of such old and metal-poor stars yields average values of $r_0 = 8.35 \pm 0.10$ kpc, $\alpha = -2.6 \pm 0.1$, $\theta = -2.6 \pm 0.2$, $z_0 = 10 \pm 2$ pc, $a \equiv 1$, $b = 0.7 \pm 0.03$, and $c = 0.6 \pm 0.03$ (within $r_{\text{bulge}} = 2.0, 2.5$, and 3.0 kpc). The results change slightly with variations of r_{bulge} in the range 2–3 kpc.

Thus the Sun is ≈ 8.3 kpc distant from the GC. The result is consistent with previous studies, whereby r_0 ranges from 7.5 to 8.9 kpc (e.g. Griv et al. 2019, table 1 therein). The finding agrees with the mean determined from numerous estimates by de Grijs & Bono (2016), 8.3 ± 0.2 (statistical error) ± 0.4 (systematic error) kpc. Bland-Hawthorn & Gerhard’s (2016) best estimate for the distance to the GC, based on various data samples, is $r_0 = 8.2 \pm 0.1$ kpc. Braga et al. (2018) obtained a distance of $r_0 = 8.46 \pm 0.03$ (stat) ± 0.11 (sys) kpc using bulge’s T2Cs. Based upon measurements of the masers and O-type stars parallaxes, Xu, Hou & Wu (2018) found $r_0 = 8.35 \pm 0.18$ kpc. This solar distance agrees closely with our estimate. The result obtained here is slightly larger than that found

Table 2. An overview of recently since 2008 derived values of z_0 .

Reference	Data used	z_0 (pc)
Jurić et al. (2008)	SDSS stars	24 ± 5
Kong & Zhu (2008)	OB and HB stars	7.6 ± 4.3
Majaess et al. (2009b)	Classical Cepheids	26 ± 3
Buckner & Froenrich (2014)	Open clusters	18.5 ± 1.2
Olausen & Kaspi (2014)	Magnestars	$13\text{--}23$
Bobylev & Bajkova (2016)	Molecular clouds	10.1 ± 0.5
	Methanol masers	5.7 ± 0.5
	H II regions	7.6 ± 0.4
Joshi et al. (2016)	Open clusters	6.2 ± 1.1
Karim & Mamajek (2017)	Disc tracer objects	17.0 ± 5.0
Yao et al. (2017)	Young pulsars	13.4 ± 4.4
Bennett & Bovy (2019)	Gaia DR2 stars	20.8 ± 0.3
Reid et al. (2019)	Molecular masers	5.5 ± 5.8
Siegert (2019)	γ -rays	15 ± 17
Skowron et al. (2019)	Classical Cepheids	14.5 ± 3.0
Cantat-Gaudin et al. (2020)	Open clusters	23 ± 3
This work	RR Lyrae stars	20 ± 2
This work	Type II Cepheids	10 ± 2

by Griv et al. (2020, 8.28 ± 0.14 kpc), which followed from an analysis of OGLE RRLs. Camarillo et al. (2018) have provided a similar value of $r_0 = 8.0 \pm 0.3$ (2σ error), namely by compiling 28 independent measurements. The value of r_0 likewise agrees with that derived by Reid et al. (2019, 8.15 ± 0.15 kpc), who modelled the space motions of molecular masers. Moreover, it is fairly consistent with conclusions by Do et al. (2019) and the Gravity Collaboration et al. (2019), who used long-spanning measurements of S2’s motion around the GC to infer $r_0 = 7.946 \pm 0.05$ (stat) ± 0.032 (sys) kpc and $r_0 = 8.178 \pm 0.013$ (stat) ± 0.022 (sys) kpc, respectively. The VERA Collaboration et al. (2020) trigonometric parallaxes and proper motions of maser sources yielded $r_0 = 7.92 \pm 0.16$ (stat) ± 0.3 (sys) kpc.

Analyses of z_0 determinations tied to O and B stars, OB associations, H II regions, horizontal branch stars, open clusters, classical Cepheids, infrared sources, molecular clouds, and other objects can be found in Karim & Mamajek (2017), Yao et al. (2017), and Siegert (2019). The offset of the Sun from the Galactic mid-plane we have found is ≈ 10 pc, again consistent with previous studies. Indeed, z_0 exhibits a range between 5 and 26 pc (Table 2). This value of the offset is close to, but somewhat lower relative to recent estimates using young pulsars and classical Cepheids (Yao et al. 2017; Skowron et al. 2019). This z_0 is above Reid et al.’s (2019) estimate but consistent within the uncertainties of estimates. It is lower than $z_0 = 23 \pm 3$ determined by Cantat-Gaudin et al. (2020) from the Gaia Data Release 2 (DR2) open clusters. Bland-Hawthorn & Gerhard

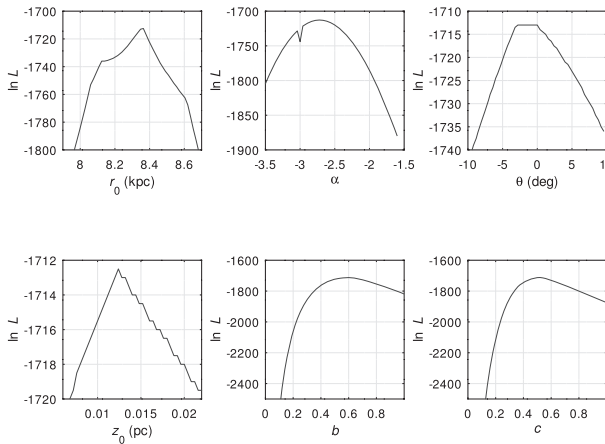


Figure 4. The natural logarithm of the likelihood L for 622 T2Cs within the Galactocentric distance $r_{\max} = 3$ kpc relative to six parameters r_0 , α , θ , z_0 , b , and c . The other parameters are held fixed in each case.

(2016) also accepted $z_0 = 25 \pm 5$ pc. It is again lower than the true median of determinations published over the past century of the Sun’s offset, $z_0 = 17 \pm 2$ pc (Karim & Mamajek 2017). Bennett & Bovy (2019) reported ‘the most precise and accurate determination’ of $z_0 = 20.8 \pm 0.3$ pc, using recent data on the positions and velocities of stars in the solar vicinity from the *Gaia* DR2 and large spectroscopic surveys. At the present, we cannot explain the $>3\sigma$ disagreement between the Bennett & Bovy (2019) and ours z_0 .

We also calculated the Sun’s height above the mid-plane for OGLE RRLs of Pietrukowicz et al. (2015). The result is $z_0 = 20 \pm 2$ pc. This newly derived distance of ours agrees well with the Bennett & Bovy (2019) result. One understands, however, that in the framework of the given treatment of astronomical observations within the power-law model it is unclear which height estimates’ is the more accurate.

Similar to OGLE RRLs, the distribution of T2Cs is ellipsoidal and slightly elongated toward the Sun ($\theta \approx -3^\circ$), with a major axis of its symmetry and two minor axes of almost the same length. The small elongation along the sightline is probably an observational bias owing to incomplete longitudinal coverage (Dékány et al. 2013). Thus the tilt angle θ is not significantly different from zero. The obtained mean ratio of the major axis to the minor axis in the plane and to the vertical axis of the ellipsoid is $\approx 1:0.7:0.6$, within the effective bulge radius of $r_{\text{bulge}} \approx 3$ kpc.

The high- $|b|$ T2Cs do not trace a strong barred structure in the direction of the bulge (cf. Griv et al. 2020). That is because both $b/a \sim 1$ and $|\theta| \sim 0^\circ$. Such a model of the bulge agrees with the Dékány et al. (2013) and Kunder et al. (2016) results, whereby old stars ($\tau \gtrsim 10$ Gyr) do not trace a strong bar but obey to a rather spheroidal distribution (see also Minniti et al. 2017; Prudil et al. 2019; Grady, Belokurov & Evang 2020, for a discussion of the problem). The latter is likely because the perturbing non-axisymmetric potential field of the bar only weakly affects an older population with high random (turbulent) velocities. Additional research on the topic is desirable.

In Fig. 4, the natural logarithm of the likelihood L is compared to each parameter for 622 T2Cs within the distance $r_{\max} = 3$ kpc from the GC. Sharp maxima of L with respect to r_0, \dots, c are apparent, which fosters a robust determination of the unknown quantities (cf. Griv et al. 2020, fig. 4 therein).

In sum, comparable parameters (r_0, \dots, c) inferred from independent OGLE and VVV samples are noteworthy. To emphasize it

again, the OGLE and VVV data analyses completed in the last two papers of a series exhibit consistent findings.

4 SUMMARY

An examination of 715 bulge T2Cs results in the following important conclusions. Findings from the optical OGLE and near-infrared VVV data are consistent within the uncertainties. A model of 3D distribution of OGLE RRLs and VVV T2Cs yields an average solar distance of $r_0 \approx 8.3$ kpc, and an exponent associated with a power law of $\alpha \approx -2.5$, within the effective bulge radius $r_{\text{bulge}} = 2.0, 2.5$, and 3.0 kpc. The results change slightly with variations of r_{bulge} in the range 2–3 kpc. The distribution of both RRLs and T2Cs in the old bulge that was formed ~ 10 Gyr ago exhibits a comparable shape of a triaxial ellipsoid, which is slightly elongated toward the Sun with a major axis of its symmetry and two minor axes of similar length. The obtained mean scale length ratio of the major axis to the minor axis in the plane and to the vertical axis of the ellipsoid within $r_{\text{bulge}} = 2\text{--}3$ kpc is $\approx 1:0.7:0.6$. The tilt angle is marginal, specifically $\theta \approx -3^\circ$. Unlike planar gas, young and intermediate-age metal-rich stars, age-old metal-poor stars do not trace a strong barred structure in the direction of the bulge at distances $r > 1$ kpc from the GC, as $b/a \sim 1$ and $|\theta| \sim 0^\circ$. Lastly, the Sun’s height from the local Galactic mid-plane is $z_0 = 10 \pm 2$ pc (while estimates obtained from an analysis of OGLE RRLs lead to $z_0 \approx 20$ pc). An inconsistency of $>3\sigma$ between estimates of z_0 from the study of T2Cs and from Bennett & Bovy’s (2019) proper investigation of recent high-precision observations is appeared. A separate study is needed to clarify the issue.

In these two parts of the work, vastly different OGLE and VVV data sets are interpreted to minimize the systematics. Looking forward, the uncertainties presented here may be improved as new observations become available. In particular, the values of r_0, \dots, c can be determined by employing the large-scale Apache Point Observatory Galactic Evolution Experiment 2 (APOGEE-2), *Gaia*-European Southern Observatory (ESO), Galactic Archaeology with HERMES (GALAH), 4-metre Multi-Object Spectroscopic Telescope (4MOST), and Large Sky Area Multi-Object Fibre Spectroscopic Telescope (LAMOST) surveys (e.g. Queiroz et al. 2020).

ACKNOWLEDGEMENTS

We would like to express our gratitude to our colleagues from the Department of Physics, Ben-Gurion University at Beer-Sheva and the Institute of Astronomy, National Tsing-Hua University at Hsin-Chu who have discussed with us many of the problems considered in the paper. The authors are grateful to Irena Zlatopolsky for her encouragement during the preparation of the paper. We also thank the anonymous referee for a useful report. The study was sponsored in part by the United States-Israel Binational Science Foundation, the Ministry of Immigrant Absorption, Israel in the framework of the program ‘KAMEA’, the Israel Science Foundation, and the Ministry of Science and Technology, Taiwan.

DATA AVAILABILITY

The stellar data underlying this paper can be downloaded via the VizieR (vizier.u-strasbg.fr) data base (Galactic Bulge Type II Cepheids NIR data, Braga+, 2019) and/or will be shared on reasonable request to the corresponding author.

REFERENCES

- Bennett M., Bovy J., 2019, *MNRAS*, 482, 1417
 Bland-Hawthorn J., Gerhard O., 2016, *ARA&A*, 54, 529
 Bobylev V. V., Bajkova A. T., 2016, *Astron. Lett.*, 42, 182
 Braga V. F., Bhardwaj A., Contreras Ramos R., Minniti D., Bono G., de Grijs R., Minniti J. H., Rejkuba M., 2018, *A&A*, 619, A51
 Braga V. F. et al., 2019, *A&A*, 625, A151
 Braga V. F. et al., 2020, *A&A*, 644, A95
 Buckner A. S. M., Froebrich D., 2014, *MNRAS*, 444, 290
 Camarillo T., Mathur V., Mitchell T., Ratra B., 2018, *PASP*, 130, 24101
 Cantat-Gaudin T. et al., 2020, *A&A*, 640, A1
 de Grijs R., Bono G., 2016, *ApJS*, 227, 5
 Dékány I., Minniti D., Catelan M., Zoccali M., Saito R. K., Hempel M., Gonzalez O. A., 2013, *ApJ*, 776, L19
 Do T. et al., 2019, *Science*, 365, 664
 Gaia Collaboration et al., 2018, *A&A*, 616, A1
 Grady J., Belokurov V., Evans N. W., 2020, *MNRAS*, 492, 3128
 Gravity Collaboration et al., 2019, *A&A*, 625, L10
 Griv E., Gedalin M., Jiang I.-G., 2019, *MNRAS*, 484, 218
 Griv E., Gedalin M., Pietrukowicz P., Majaess D., Jiang I.-G., 2020, *MNRAS*, 499, 1091
 Joshi Y. C., Dambis A. K., Pandey A. K., Joshi S., 2016, *A&A*, 593, A116
 Jurić M. et al., 2008, *ApJ*, 673, 864
 Karim M. T., Mamajek E., 2017, *MNRAS*, 465, 72
 Kong D. L., Zhu Z., 2008, *Acta Astron. Sinica*, 49, 224
 Kunder A. et al., 2016, *ApJ*, 821, L25
 Majaess D., 2010, *Acta Astron.*, 60, 55
 Majaess D., Turner D., Lane D., 2009a, *Acta Astron.*, 59, 403
 Majaess D. J., Turner D. G., Lane D. J., 2009b, *MNRAS*, 398, 263
 Majaess D. J., Dékány I., Hajdu G., Minniti D., Turner D., Gieren W., 2018, *Ap&SS*, 363, 127
 Minniti D. et al., 2010, *New Astron.*, 15, 433
 Minniti D. et al., 2017, *AJ*, 153, 179
 Navarro M. G., Minniti D., Capuzzo-Dolcetta R., Alonso-García J., Contreras Ramos R., Majaess D., Ripepi V., 2021, *A&A*, 646, A45
 Olausen S. A., Kaspi V. M., 2014, *ApJS*, 212, 6
 Pietrukowicz P., 2020, in Valluri M., Sellwood J. A., eds, Proc. IAU Symp. Vol. 353, *Galactic Dynamics in the Era of Large Surveys*. Cambridge Univ. Press, Cambridge, p. 1
 Pietrukowicz P. et al., 2015, *ApJ*, 811, 113
 Prudil Z., Dékány I., Catelan M., Smolec R., Grebel E. K., Skarka M., 2019, *MNRAS*, 484, 4833
 Queiroz A. B. A. et al., 2020, *A&A*, 638, A76
 Rastorguev A. S., Pavlovskaya E. D., Durlevich O. V., Filipova A. A., 1994, *Astron. Lett.*, 20, 591
 Reid M. J. et al., 2019, *ApJ*, 885, 131
 Siegert T., 2019, *A&A*, 632, L1
 Skowron D. M. et al., 2019, *Science*, 365, 478
 Soszyński I. et al., 2014, *Acta Astron.*, 64, 177
 Soszyński I. et al., 2019, *Acta Astron.*, 69, 321
 Surot F. et al., 2019, *A&A*, 629, A1
 VERA Collaboration et al., 2020, *PASJ*, 72, 50
 Xu Y., Hou L.-G., Wu Y.-W., 2018, *Res. Astron. Astrophys.*, 18, 146
 Yao J. M., Manchester R. N., Wang N., 2017, *MNRAS*, 468, 3289

This paper has been typeset from a TeX/LaTeX file prepared by the author.